Shock pressures induced in condensed matter by laser ablation

Damian C. Swift* and Thomas E. Tierney IV

P-24 Plasma Physics, Los Alamos National Laboratory, MS E526, Los Alamos, New Mexico 87545, USA

Roger A. Kopp

X-1, Los Alamos National Laboratory, MS B259, Los Alamos, New Mexico 87545, USA

J. Tinka Gammel

T-1, Los Alamos National Laboratory, MS B221, Los Alamos, New Mexico 87545, USA

The Trident laser was used to induce shock waves in samples of solid elements, with atomic numbers ranging from Be to Au, using pulses of 527 nm light around 1 ns long with irradiances of the order of 0.1 to 10 PW/m^2. States induced by the resulting ablation process were investigated using laser Doppler velocimetry to measure the velocity history of the opposite surface. By varying the energy in the laser pulse, relations were inferred between the irradiance and the induced pressure. For samples *in vacuo*, an irradiance constant in time does not produce a constant pressure. Radiation hydrodynamics simulations were used to investigate the relationship between the precise pulse shape and the pressure history. In this regime of time and irradiance, it was possible to reproduce the experimental data to within their uncertainty by including conductivity-dependent deposition of laser energy, heat conduction, gray radiation diffusion, and three temperature hydrodynamics in the treatment of the plasma, with ionizations calculated using the Thomas-Fermi equation. States induced in the solid sample were fairly insensitive to the details of modeling in the plasma, so Hugoniot points may be estimated from experiments of this type given a reasonable model of the plasma. More useful applications include the generation of dynamic loading to investigate compressive strength and phase transitions, and for sample recovery.

I. INTRODUCTION

Investigation of the response of materials to dynamic loading—such as the equation of state (EOS) and strength—relies on experiments in which a well-characterized load is applied and the response is measured. Most of these experiments have employed shock waves, induced by projectile impact or the detonation of chemical explosives [1,2]; these experiments typically explore the response on microsecond time scales at pressures between ~0.1 and 100 GPa. Higher pressure experiments have been performed in which the shock wave was generated using the x-ray radiation from a nuclear explosion [3,4]; more recently, laser-driven hohlraums have been used as a source of x-ray drive for conceptually similar experiments [5–7]. In all these cases, the momentum and energy associated with the shock in the sample are far less than the overall quantities in each experiment. As a result, it is at best difficult to recover the sample for subsequent investigation of the microstructure, and there are often serious concerns about artifacts introduced by complicated loading paths as the sample is brought to rest.

In the experiments described here, laser energy was used to induce a shock wave in solid samples by irradiating the sample surface directly. At the start of the laser pulse, energy is deposited in the skin depth at the surface of the sample; material at the surface ablates as plasma in which subsequent laser energy is deposited. Reaction and plasma pressure apply loading to the remaining material in the sample. The loading experienced by the sample is often less simple than that induced by the impact of an initially cold flyer plate, so the technique is arguably less appropriate for high accuracy measurements of EOS points. However, we have found laser-induced loading to be perfectly adequate for studies of phenomena which can be observed around the rising edge of the shock wave, including plasticity and phase changes. "Collateral" momentum and energy in the loading system were insignificant in the experiments described here—in comparison, for instance, with the sabot used in a gas gun or the detonation products and casing in explosively driven systems—so sample recovery was relatively straightforward.

Laser-driven shock waves have been used previously to measure the EOS at high pressure (~1 to 10 TPa) [5,7]. In contrast, the work described here includes a systematic study of the relationship between the laser irradiance and the pressure of the resulting shock wave, for elements ranging from Be to Au, and pressures up to a few tens of gigapascals. This pressure range is better suited to investigations of constitutive behavior and solid-solid phase transitions. Radiation hydrodynamics simulations are also discussed, and a calculational method reported which reproduces the experimental results to within their uncertainty and can thus be used to predict the loading history experienced at each point in the sample, for arbitrary irradiance profiles in the regime explored by the experiments.

The present paper covers systematic trends in ablation-induced pressures for different materials and irradiances. De-

*Electronic address: dswift@lanl.gov
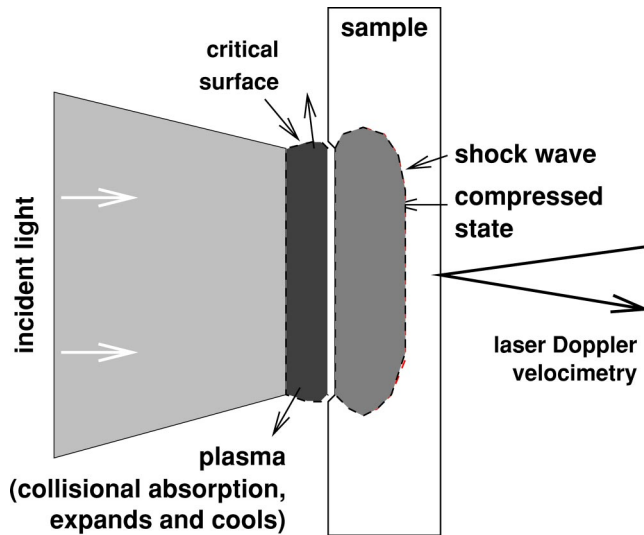URL: http://public.lanl.gov/dswift

FIG. 1. Schematic cross section of laser drive experiments. The sample is typically a few tens of microns thick; focal spot is 5 mm in diameter.

tailed interpretation of the loading induced in each experiment is given by outline and example only; more complete descriptions of the loading and response applied in individual experiments will be published separately by material.

II. DIRECT DRIVE EXPERIMENTS

Experiments were performed using the Trident facility at Los Alamos, operating in nanosecond mode at 527 nm wavelength (green). Trident is a neodymium-glass laser with a fundamental wavelength of 1054 nm. In each experiment, the planar sample was irradiated on one side over a region 5 mm in diameter, and the velocity history was measured on the opposite side (Fig. 1).

A. Sample configuration

Samples were in the form of foils or crystals, typically a few tens of microns thick and 5 to 10 mm across. In most cases both surfaces were free, though experiments were also performed with release windows made of sapphire, LiF, or PMMA; experiments included combinations in which the shock impedance of the window was both higher and lower than that of the sample. Samples were mounted in a reusable clamp, attached to the Trident target positioning system (Fig. 2).

Materials investigated included Be, Al, Si, Fe, Ga, Sn, Ta, and Au; results are presented here for Be, Fe, Sn, and Au. All samples were in the form of rolled foils, except for Si [crystals in the (100) orientation] and Ga (crystals of unknown orientation). Be samples included foils and crystals cut along (0001) planes. Some of the experiments were performed in support of other projects rather than as dedicated studies of the irradiance-pressure relation, so the temporal profile of the laser pulse and the quality of the velocimetry records were not necessarily optimized for the measurements considered here; thus some of the uncertainties are larger than can be
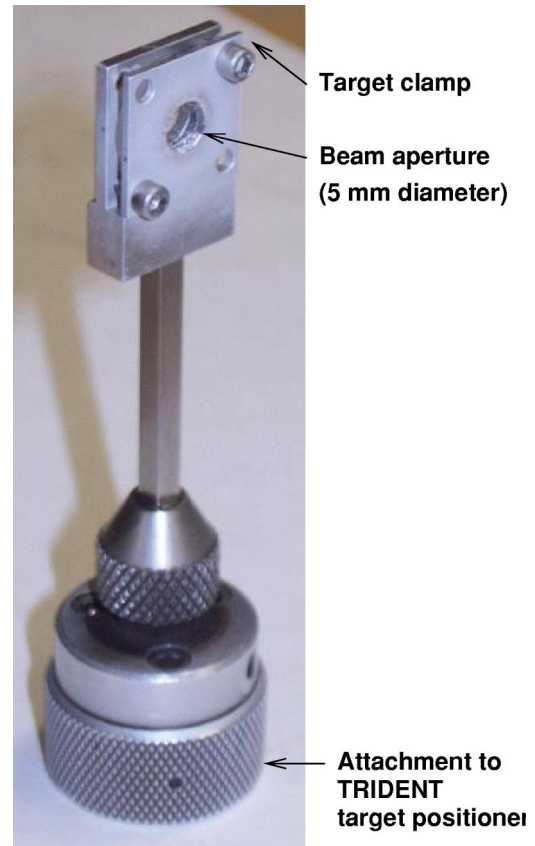

FIG. 2. Photograph of sample holder assembly.

achieved with the laser and diagnostic configurations available at Trident.

All of the materials were nominally pure, and unless otherwise stated were obtained from Goodfellow Corp. and of the highest purity offered. The Be crystals were cut from a single crystal boule grown at Los Alamos. Some of the Be, Al, and Fe foils were obtained from Research Metals, Inc.

B. Laser drive

The Trident master oscillator was operated in nanosecond mode, in which the pulse delivered to the target was composed of up to thirteen elements of 180 ps duration. The intensity of each element is controlled independently, allowing considerable flexibility in controlling the irradiance history. In some experiments, the composite pulse was split and recombined as two consecutive pulses with different relative amplitudes, allowing the maximum pulse length to be doubled. For dynamic loading experiments, the infrared pulse was frequency doubled to 527 nm (green) to improve the coupling efficiency to matter. At this wavelength, the two main beams could each deliver up to ~250 J, and the third beam up to ~50 J. One of the main beams was used to drive the samples.

The raw drive beam from Trident had significant spatial variation across the beam. A Fresnel zone plate was used to distribute the laser energy more uniformly across the sample. As designed, this diffractive optical element would convert a perfectly focused spot to a disc of 4 mm diameter containing

85% of the laser light (with the remaining energy contained in higher-order rings further from the center of the disc). However, undiffracted light produced a hotspot at the center of the disc. The final focusing lens was shifted 6 mm from best focus to eliminate the hotspot; this produced a disc 5 mm in diameter. The defocusing process introduced a very slight spatial variation in irradiance, but this was not found to introduce any measurable variation in shock pressure.

The total energy and irradiance history were measured on each shot by extracting 4% of the laser drive from transmission through an uncoated mirror, and recording with a calorimeter and a photodiode. The total pulse energy was usually determined to ±1 J. The conversion factor between the nominal drive energy and the energy delivered to the sample has been calibrated from time to time; in effect it represented a systematic uncertainty which remained constant usually for the whole of a series of experiments.

C. Surface velocimetry

The velocity history of the surface opposite the irradiated side was measured by laser Doppler velocimetry, using an imaging interferometer of the Visar type [8]. Spatially distributed interference fringes were set up, and their motion recorded using one or two optical streak cameras. A pulsed 660 nm laser provided illumination for the Visar.

Experiments were performed with various different magnifications, the field of view varying between 500 and 4000 μm and the spatial resolution of the imaging system between 10 and 100 μm. The streak camera slit was generally set to 300 μm, equivalent to 100 μm on the 25 mm photocathode. The time window of the streak cameras was 16 or 37 ns, giving a nominal time resolution of 50 or 100 ps. In principle, the absolute time offset between the drive pulse and the Visar record may be determined to 100 ps or better, as the streak camera was triggered by signals from the master oscillator. In practice, from a combination of equipment jitter and procedural difficulties, there were occasional uncontrolled timing changes of up to 1 ns during the earlier experiments. In later series of shots, timing fiducial pulses 2 ns apart were fed directly to the slit of streak camera; the first pulse was synchronized carefully with respect to the drive pulse, providing absolute time calibration to better than 100 ps on each shot.

The velocity sensitivity was varied between 800 m/s fringe and 5 km/s fringe. The fringe pattern was converted to velocity by following the extrema as a function of time; velocity changes were thus multiplexed with position. Velocities were inferred at constant positions on the surface by interpolating between extrema. Typical velocity uncertainties were ~5% for an individual fringe, dominated by camera noise and diffraction rings in the optical path, which limited the accuracy of the fringe-following algorithm. The accuracy was improved by smoothing over adjacent fringes or temporal slices. Smoothing functions allowed linear variation in space or time, so the temporal resolution was not reduced significantly by this process. At 800 m/s fringe, the time delay for light arriving through the slow leg of the interferometer was 0.4 ns, so care was taken when attempting to
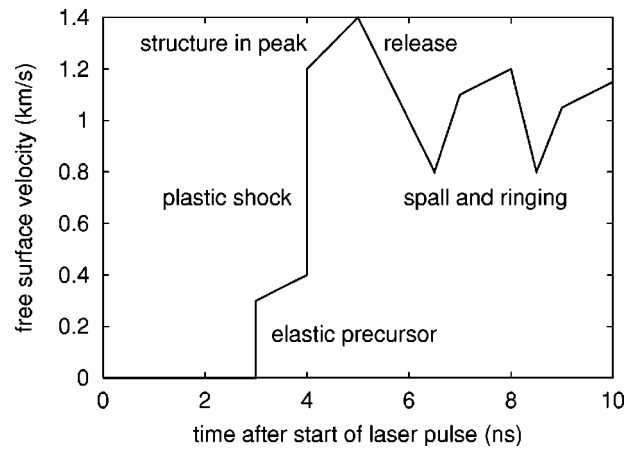

FIG. 3. Schematic velocity history for laser drive experiments.

interpret subnanosecond features with this étalon. The effective temporal resolution of the velocity record depended on the nature of any given feature. The arrival time of the first velocity disturbance could typically be identified to within 2 to 3 pixels. The resolution of temporal wave profiles depended on the quality of the individual streak camera records (signal and noise levels, presence and size of any spatial speckles or interference patterns from the optical system, one-dimensionality of the wave), which affected the degree of smoothing introduced in the fringe analysis. In the results presented here, the temporal resolution of velocity histories was dominated by the inherent response time of the interferometer, and the temporal resolution of peak or average velocities was incorporated as part of the quoted uncertainty.

Experiments were performed with a variety of different magnifications and spatial resolutions. The spatial resolution of the complete optical system was measured directly in some cases by capturing images of sharp edges and gratings. The results presented here were all obtained from planar experiments, so the precise spatial resolution is not important.

D. Velocity histories and data reduction

Schematic velocity histories consisted of an elastic precursor, the main plastic shock wave, and release with spall reverberations. The main shock wave generally exhibited temporal variations in velocity, the details depending on the precise laser irradiance history. For any given material, if the drive pressure was high enough the elastic precursor was absent. If the drive pressure was very low, the transmitted wave was entirely elastic (Fig. 3).

In these experiments, elastic precursors were generally significantly stronger than have been observed in the same materials on microsecond time scales, indicating higher flow stresses [9]. This difference reflects the combined effect of time dependence in plastic flow and texture and initial plastic work arising from the use of rolled foil samples. For almost all shots, the arrival and magnitude of the shock wave were one-dimensional (1D) to the temporal and velocity accuracy of the Visar data. Departures from 1D shock arrival occurred when the alignment of the Visar and drive beam had drifted with respect to each other. In some cases, particularly for higher energy experiments, the fringe contrast decreased af-
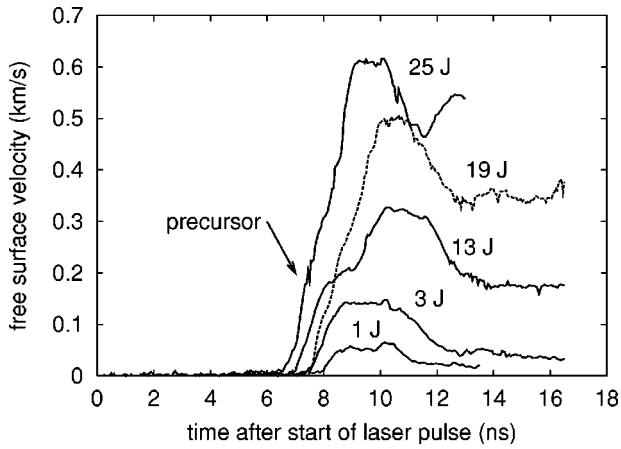
FIG. 4. Example velocity histories for Sn foils 25 μm thick, as a function of total laser drive energy.

FIG. 6. Irradiance-pressure relations deduced from measured free surface velocity: Fe and Sn. The uncertainty shown for mean irradiance includes the uncertainty in measured energy, and also the variation of irradiance during the pulse. The uncertainty in pressure was calculated from the measurement uncertainty in velocity, assuming the EOS was exact.

ter the passage of the main shock. This probably indicates spatial variations in velocity, which were likely caused by spall and breakup seeded by the microstructure of the samples.

Two forms of analysis and interpretation were used. To provide a simple measure of the relationship between irradiance and pressure, the mean irradiance was calculated using the measured pulse energy over the nominal pulse duration, and was compared with a mean pressure calculated given the EOS of the material and relating the peak free surface velocity (Fig. 4) to the shock pressure. For plastic shocks of a few tens of gigapascals or less, the bulk particle velocity was estimated by halving the free surface velocity; the pressure was then calculated from the shock Hugoniot in pressure-particle speed space. The points for each material defined a fairly clear locus; in log space the loci for different materials had similar slopes but different intercepts (Figs. 5 and 6).

For a given material and drive pressure, there is a maximum sample thickness over which the shock wave is fully
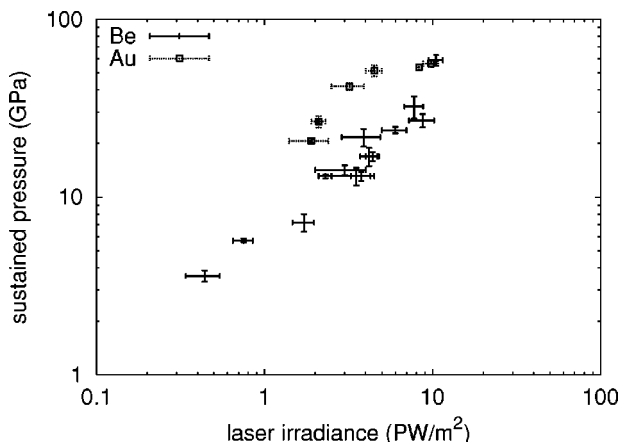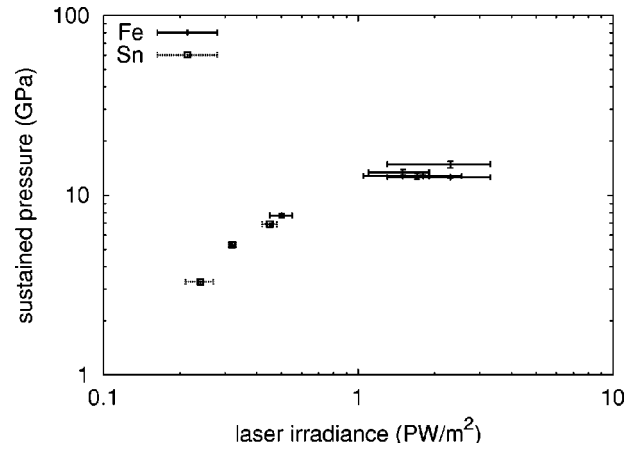
supported, i.e., until the rarefaction following the shock catches up with it and erodes the peak shock pressure before the shock reaches the opposite surface of the sample. Some of these experiments included thick samples and hence decaying shocks. The decrease in the peak pressure just inside the free surface was ~10% or less; experiments with thick samples tended to fall below the locus of pressure-irradiance measurements formed by experiments on thinner samples.

III. RADIATION HYDRODYNAMICS

Laser-matter interaction is a nonlinear and time-dependent process: a constant laser irradiance generally does not induce a constant pressure in the sample. To interpret laser-driven experiments, radiation hydrodynamics simulations were used to simulate the pressure history experienced as a function of position in the sample and of irradiance history. Depending on the time scales and irradiance, many physical processes may need to be included to reproduce laser-matter interactions accurately. However, in the regime explored by these experiments (picosecond to nanosecond time scales, laser irradiance ~0.1 to 10 PW/m^2), previous experience using the LASNEX radiation hydrocode [10] suggested that laser ablation and dynamic loading could be simulated accurately by assuming three temperature hydrodynamics (ions, electrons, and radiation), allowing thermal conduction and radiation diffusion, and calculating the absorption of the laser energy in the expanding plasma cloud through the electrical conductivity. This model was needed only for material ablated by the laser: a region ~1 μm wide of the solid sample, and the resulting plasma cloud. The remainder of the condensed phase could be treated using non-radiative continuum mechanics, i.e., with an EOS plus a constitutive model when elasticity and strength were significant. Some specific processes excluded in this plasma model include resonant absorption, transport of the resulting hot electrons, and generation, transport, and deposition of Bremsstrahlung x rays.
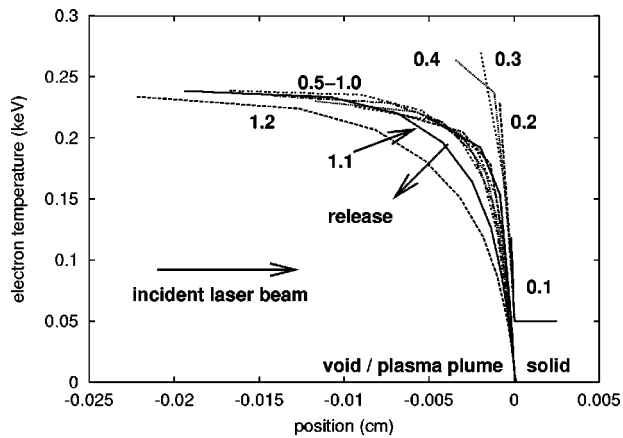

FIG. 5. Irradiance-pressure relations deduced from measured free surface velocity: Be and Au. The uncertainty shown for mean irradiance includes the uncertainty in measured energy, and also the variation of irradiance during the pulse. The uncertainty in pressure was calculated from the measurement uncertainty in velocity, assuming the EOS was exact.

FIG. 7. Temperature profiles in expanding plasma predicted by radiation hydrodynamics simulations during ablation of Fe by a laser pulse of 10 PW/m², lasting for 1 ns. Numbers are profile times after start of laser pulse, in nanoseconds.

FIG. 8. Profiles of mass density predicted by radiation hydrodynamics simulations during ablation of Fe by a laser pulse of 10 PW/m², lasting for 1 ns. Numbers are profile times after start of laser pulse, in nanoseconds.

Simulations for all the materials tested were performed using the HYADES radiation hydrocode, version 01.05.11 [11]. This hydrocode used a 1D Lagrangian discretization of the material, and leapfrog time integration, and did not include material strength in the solid sample. Shock waves were stabilized using artificial viscosity. The EOS were taken from the SESAME database [12]; these were tables covering a wide range of states from compressed condensed matter to plasma, though the accuracy was not necessarily high or known. Opacities for radiation diffusion were also taken from SESAME. Conductivities for laser deposition and heat conduction were calculated using several different ionization models: Saha, Thomas-Fermi, and average atom [11–13]. With the Saha ionization model, the irradiance-pressure relation fell below the experimental data for elements of higher atomic number Z, also becoming worse for higher irradiances. With Thomas-Fermi ionization, the simulations matched the data for all elements and irradiances considered. The flux limiter was set to 0.03 of the free stream value—a common choice for simulations of this type [14].

The initial spatial mesh was set up to be expanding, to allow adequate resolution of the material to be ablated. Moving away from the sample surface, adjacent cells were expanded by 5%. The cell closest to the surface was 5 nm wide. Sensitivity studies were performed to determine the mesh resolution necessary for converged calculations. Although the states in the plasma were relatively sensitive to the resolution, the states in the solid material had converged at a lower resolution.

A. Constant irradiance

Simulations were performed applying a constant irradiance to the sample for 1 ns. The irradiance was ramped up and down over 0.1 ns to maintain stability in the simulations.

The simulations showed the plasma layer expanding from the surface. After the first ~0.2 ns, the profile of the plasma was close to a steady state. The critical surface was predicted to lie approximately 0.5 μm from the sample surface. This was very close compared with the diameter of the laser spot,
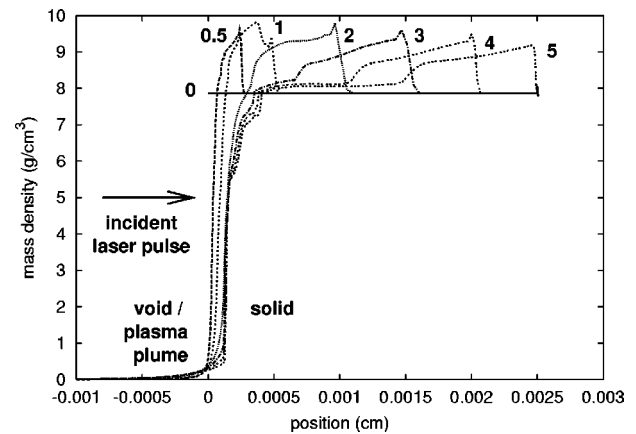
so 2D effects from the lateral expansion of the plasma plume should be negligible. After the end of the laser pulse, the plasma close to the surface expanded and cooled rapidly (Fig. 7). The pressure exerted on the cold material exhibited an initial spike, followed by a stage of more constant pressure, corresponding to the steady profile in the plasma. The compression in the sample exhibited analogous features (Fig. 8). The spike decayed as the shock wave crossed the sample; the spike was caused partly by the numerical representation of the shock in the expanding mesh.

The constant irradiance simulations were reduced to irradiance-pressure relations by selecting the pressure generated during the steady-state phase of the plasma expansion, immediately following the initial pressure spike (Fig. 9). The pressure in this region was not perfectly constant, so there was an uncertainty associated with the data reduction. The uncertainty was generally greater for materials of higher Z, suggesting that the irradiance should generally be made to ramp up more steeply with time in order to induce a constant pressure, to an extent increasing with Z.

Apart from Be and Al, the irradiance-pressure curves for the different elements exhibited distinct steps and changes of
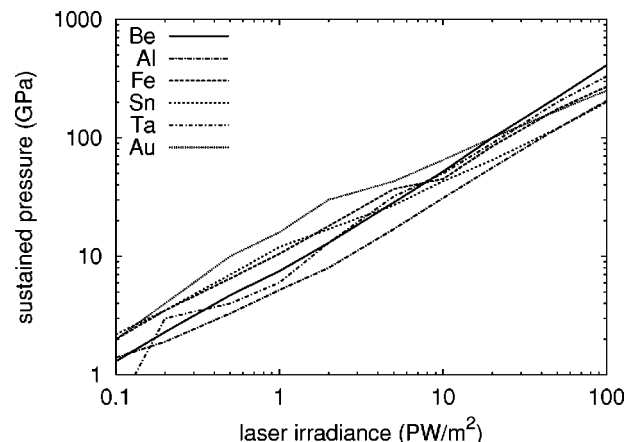

FIG. 9. Irradiance-pressure relations deduced from radiation hydrodynamics simulations.
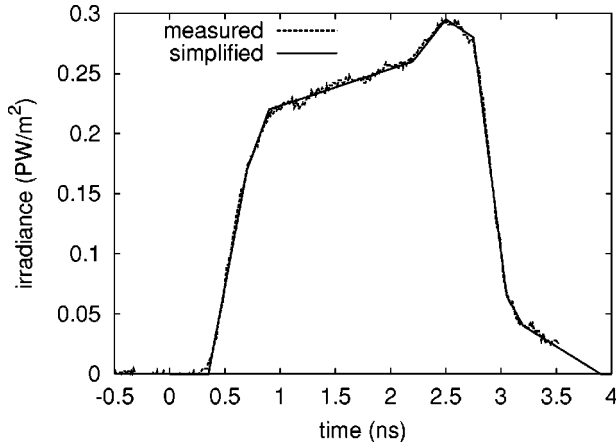
FIG. 10. Example of measured irradiance history and simplified history used for radiation hydrodynamics simulations (Trident shot 14 962: 25 μm Sn). Measured history has not been corrected for pulse to start at time zero.

FIG. 11. Example of pressure history predicted 1 μm from the ablation surface using radiation hydrodynamics and simplified pressure used as boundary condition for continuum mechanics simulation (Trident shot 14 962: 25 μm Sn).

gradient in the regime considered. These appeared to correspond to the ionization of deeper electron shells of atoms in the plasma, which became hotter at higher irradiance. Similarly, the flattening of the curves at higher irradiance and specifically above the ionization steps appeared to be caused by the higher specific heat capacity and conductivity of the plasma at higher ionization states: more power was needed to increase the pressure than at lower pressures. Irradiance-pressure relations are commonly assumed to follow a power law:

$$p = \alpha I^{\beta}, \quad (1)$$

where p is the pressure and I the irradiance. The simulations indicate that, although this form is not valid in general over multiple decades of irradiance and pressure, it is reasonable to represent the relation with an exponential over one decade or so. By inspection, a representative value for the exponent β was $\frac{2}{3}$ for all elements and irradiances considered. Locally, values closer to unity were found and also correspondingly smaller values elsewhere.

B. Simulations using measured irradiance history

Some calculations were performed using the irradiance history measured on individual shots to simulate the precise loading history applied to each sample. The raw photodiode record was converted to irradiance by scaling so that the integral under the curve matched the measured pulse energy, and dividing by the area of the focal spot. The raw record contained high frequency fluctuations, giving negative apparent values of the irradiance when the signal was low. For the simulations, the inferred irradiance history was reduced to a piecewise linear variation reproducing the principal features to a few percent in irradiance (Fig. 10).

For experiments in which the strength of the material significantly affected the shock propagation and hence the free surface velocity history, the pressure history was extracted from the radiation hydrodynamics simulation near the irradiated surface and was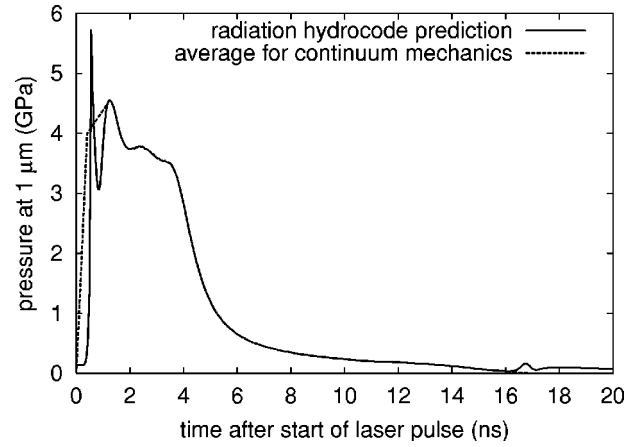 used as an applied pressure boundary condition for continuum mechanics simulations omitting radiation transport. The point used for extracting the pressure history was Lagrangian—i.e., following an element of material rather than a fixed position in space—and was chosen to be close to the irradiated surface but sufficiently deep inside not to be ablated. An initial depth of 1 μm was chosen for most simulations. The continuum mechanics program was LAGC1D version 5.2, using a 1D Lagrangian discretization of the material, predictor-corrector (second order Runge-Kutta) time integration, and artificial viscosity to stabilize shock waves [15]. In some cases the pressure history predicted using radiation hydrodynamics exhibited numerical oscillations close to the ablation surface, caused by the ablation of successive meshes of material more quickly than heat transport was able to redistribute energy and thus smooth the solution. These were averaged out in a way analogous to the simplification of the irradiance history when constructing the applied pressure boundary condition to apply to the nonradiation simulation (Fig. 11).

As direct laser irradiation is a relatively novel loading technique, and as these experiments explore shorter time scales and use thinner samples prepared differently than are usual for shock wave experiments, it is illustrative to compare the experimental data with simulations as different parts of the material response are included. For shocks significantly stronger than the flow stress, the peak free surface velocity was generally reproduced to within a few percent by simulations which neglected the strength of the sample. If the shock was strong enough to overdrive the elastic precursor, the agreement was often better, as one would expect for regimes in which the response is dominated by the scalar equation of state (pressure) over the elastic component (which is limited by the flow stress). A treatment of spall was needed to give a reasonable match to the release part of the velocity history, ensuring that the velocity did not decrease to close to zero but remained larger as a layer of the sample was ejected from the bulk (Fig. 12).

The inclusion of elasticity and flow stress generally made the agreement better. As a consequence of the texture of the
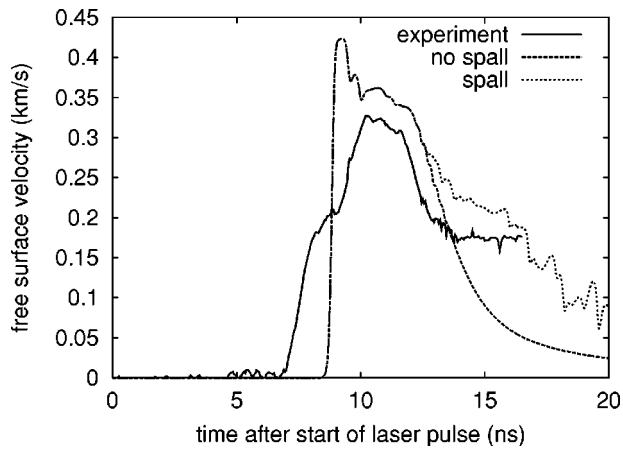
FIG. 12. Example free surface velocity histories predicted using EOS and spall models in the solid sample but no strength model (Trident shot 14 962: 25 μm Sn). Omitting a strength model, the peak velocity exhibits a spike. Otherwise, the gradient around the peak velocity is reproduced fairly well.

samples (rolled foil or single crystal) and the short time scales compared with gas gun experiments, elastic precursors tended to be significantly stronger than would be predicted using strength models calibrated to data taken on microsecond time scales [9]; strong precursors were observed in Be and Fe [16–18]. It was possible to reproduce the amplitude of the elastic precursor by increasing the flow stress, but in some cases this made the agreement around the peak surface velocity significantly worse if applied in too simplistic a strength model. The detailed constitutive behavior of materials on these time scales will be discussed elsewhere. (See Fig. 13.)

IV. IRRADIANCE-PRESSURE RELATIONS

By reducing the results of radiation hydrodynamics simulations with a constant irradiance as described above, the predicted irradiance-pressure relation can be compared with the experimental measurements over a wide range of irradi-

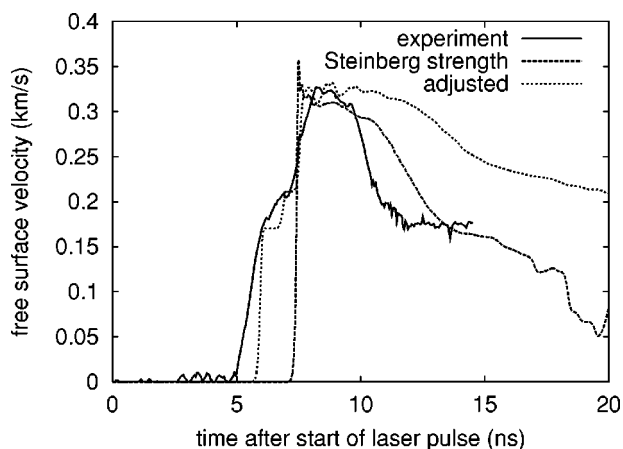FIG. 13. Example free surface velocity histories predicted using different constitutive models for the solid sample (Trident shot 14 962: 25 μm Sn).
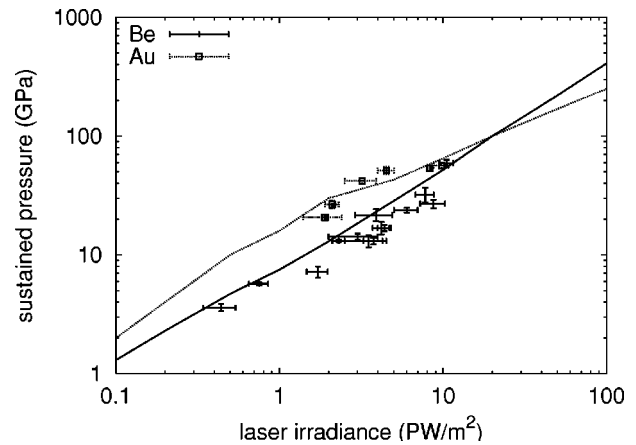

FIG. 14. Comparison between measured irradiance-pressure points and radiation hydrodynamics predictions: Be and Au.

ance and material. The predictions reproduced the magnitude and trend of the experimental data quite well, for variations in irradiance and Z. In many cases, the difference between calculation and experiment was within the nominal uncertainty in the experimental measurement. In almost all cases, the difference was within twice the nominal uncertainty. Given that the simulations were reduced by choosing a representative ablation pressure for the quasisteady regime, this difference is unlikely to represent inadequacy in the physical model used for the simulations. Considering the complete data set, there was no evidence that the irradiance deduced by calorimetry and photodiode measurements was in error by more than a few percent (Figs. 14 and 15).

Some of the Be data fell significantly below the predicted irradiance-pressure relation (Fig. 14). These experiments used foils 50 and 125 μm thick, and the rarefaction following the end of the laser pulse was able to erode the peak shock pressure before it could be observed by velocimetry. Omitting radiation transport made the agreement substantially worse (Fig. 16); alternative ionization models such as Saha and average atom made little difference to the simulations.
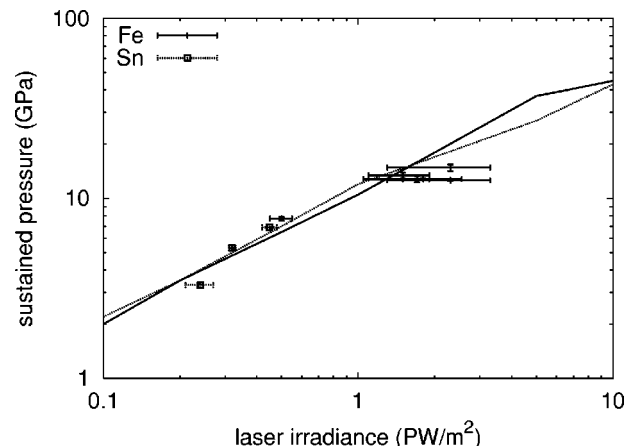

FIG. 15. Comparison between measured irradiance-pressure points and radiation hydrodynamics predictions: Fe and Sn.
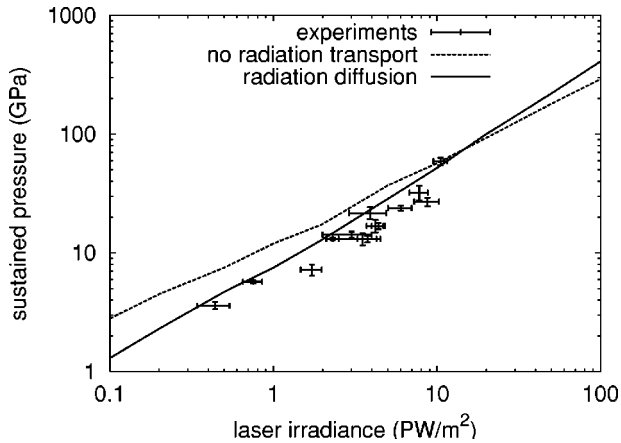
FIG. 16. Effect of omitting radiation transport from radiation hydrodynamics predictions of irradiance-pressure relation for Be.

V. DISCUSSION

The irradiance-pressure relations developed here by experiment and simulation are a convenient way to represent the effectiveness of laser ablation for generating pressures on nanosecond time scales in different materials. Ablation using a constant laser irradiance does not generally induce a constant pressure, so this representation of ablation has an inherent uncertainty.

Since it is necessary to tailor the irradiance history in order to induce a constant pressure drive, a constant ablation pressure can be produced by intention only to the accuracy with which the irradiance history can be controlled. At Trident in its current configuration, this is equivalent to a few percent in pressure, if several shots can be fired to tune in the laser gain. The pressure may fortuitously be constant to a higher accuracy, in which case surface velocimetry can measure the constancy.

Even with a drive pressure varying on the order of 100%, ablative loading nonetheless seems useful for investigating the response of materials to dynamic loading. For solid samples tens to hundreds of microns thick, loaded for a few nanoseconds at pressures up to tens of gigapascals, the decay of the shock caused by the rarefaction following the end of the laser pulse typically eroded the peak pressure by a few tens of percent or less, and had little or no effect on elastic waves, in the materials investigated. The speed and amplitude of the elastic precursor were measured, as was the shape of the velocity history between the precursor and the plastic shock. These data provide a large amount of information on the flow stress under dynamic loading, to similar accuracy as can be achieved from impact experiments. Similarly, phase transitions occurring on the rising edge of the shock wave can be characterized, e.g., by the splitting of the shock wave into the wave of maximum compression in the starting phase, followed by a phase transition wave to the peak pressure. Even if the peak pressure varies as a result of the irradiance history used, the phase transition pressure and rate information can be deduced quite accurately from the velocity history around the resulting features in the shock wave. Finally, if simulations of the pressure history induced by the irradiance history can be trusted—as has been demonstrated

here for elements—then the stress history experienced at each position through the sample can be predicted by radiation hydrodynamics and continuum mechanics to ~1% in stress. Thus the microstructure of recovered samples can be related to the loading history in a meaningful way. Nonconstant shocks are also relevant to investigations of the performance of materials when loaded by other methods, e.g., the decaying waves induced by detonation waves in chemical explosives [19].

A varying pressure drive can be used to generate a constant pressure by using phase transitions with a negative volume change: if the varying drive lies above the phase transition pressure but does not overdrive it, the shock wave to the maximum pressure in the starting phase travels faster than the shock to the maximum pressure, so a region of constant pressure is produced. The varying drive makes itself felt later in time, so this method is not well suited to high accuracy measurements of the release following the shock. The applicability is also limited by the need to select materials with suitable phase transformations.

VI. CONCLUSIONS

Experiments were performed exploring the pressure generated in a variety of elements tens of microns thick, by laser ablation at 527 nm with pulses around 1 ns long and of irradiance around 0.1 to 10 PW/m^2. The pressure was deduced from the peak free surface velocity, measured at the side opposite the ablation using laser Doppler velocimetry, and assuming the equation of state. Pressures ranged up to a few tens of gigapascals. In this regime, no problems were observed associated with the use of laser ablation to induce loading: x-ray preheat, obscuration of optical diagnostics by hot electrons or clouds of plasma, and conduction effects in the condensed sample were all negligible.

Radiation hydrodynamics simulations were able to reproduce the overall trend of the irradiance-pressure relations, using three temperature hydrodynamics for the plasma region, heat conduction, radiation diffusion, and Thomas-Fermi ionization. Using the measured irradiance-time history from each experiment, the detailed velocity history at the free surface was reproduced to within the uncertainty in irradiance, velocity, and material properties. The velocity histories were sensitive to the equation of state, elasticity, flow stress, spall strength, and phase transitions; these phenomena can thus be investigated at least in principle using laser ablation to induce dynamic loading.

[1] S.P. Marsh, *LASL Shock Hugoniot Data* (University of California, San Francisco, 1980).

[2] B. van Thiel, Lawrence Radiation Laboratory Report No. UCRL-50108, 1966 (unpublished).

[3] R.F. Trunin, *Shock Compression of Condensed Materials* (Cambridge University Press, London, 1998).

[4] C.E. Ragan III, Phys. Rev. A **21**, 458 (1980).

[5] D. Batani, A. Balducci, D. Beretta, A. Bernardinello, T. Lower, M. Koeing, A. Benuzzi, B. Faral, and T. Hall, Phys. Rev. B **61**, 9287 (2000).

[6] S.D. Rothman, A.M. Evans, P. Graham, C.J. Horsefield, and T. Jalinaud, J. Phys. D **35**, 3021 (2002).

[7] A. Benuzzi-Mounaix, M. Koenig, G. Huser, B. Faral, D. Batani, E. Henry, M. Tomasini, B. Marchet, T.A. Hall, M. Boustie, T. de Rességuier, M. Hallouin, F. Guyot, D. Andrault, and T. Charpin, Phys. Plasmas **9**, 2466 (2002).

[8] L.M. Barker and R.E. Hollenbach, J. Appl. Phys. **43**, 4669 (1972).

[9] D.J. Steinberg, Lawrence Livermore National Laboratory Report No. UCRL-MA-106439 change 1, 1996 (unpublished).

[10] G.B. Zimmermann and W.L. Kruer, Comments Plasma Phys. Controlled Fusion **2**, 51 (1975).

[11] Documentation for HYADES computer program, version 01.05.11, Cascade Applied Sciences Inc., Golden, Colorado, 1998.

[12] S.P. Lyon and J.D. Johnson, Los Alamos National Laboratory (private communications on SESAME database).

[13] Ya.B. Zel'dovich and Yu.P. Raizer, *Physics of Shock Waves and High Temperature Hydrodynamic Phenomena* (Academic Press, New York, 1966).

[14] R. Dendy, *Plasma Physics* (Cambridge University Press, Cambridge, 1993).

[15] Documentation for LAGC1D computer program, version 5.2 (incorporating ARIADNE material properties library, version 6.2, and C++ mathematical class library, version 1.1), Wessex Scientific and Technical Services, Ltd., Perth, Scotland, 2002; URL http://www.wxres.com.

[16] D.C. Swift, D.L. Paisley, G.A. Kyrala, and A. Hauer, in *Shock Compression of Condensed Matter-2001*, edited by M.D. Furnish *et al.*, AIP Conf. Proc. No. 620 (Melville, New York, 2002), pp. 1192–1195.

[17] D.C. Swift, D.L. Paisley, and M.D. Knudson, LANL Report No. LA-UR-03-5219 (unpublished).

[18] J.T. Gammel, D.C. Swift, and T.E. Tierney IV, LANL Report No. LA-UR-03-7710 (unpublished).

[19] A.V. Bushman, G.I. Kanel', A.L. Ni, and V.E. Fortov, *Intense Dynamic Loading of Condensed Matter* (Taylor and Francis, Washington, D.C., 1993).